Electrochemical Deposition of Fe-S-O Thin Films

Kai Yang[1*], Shoichi Kawai[2], and Masaya Ichimura[1]

1. Department of Engineering Physics, Electronics and Mechanics, Nagoya Institute of Technology, Gokiso-cho, Showa-ku, Nagoya, 466-8555, Japan

2. DENSO CORP. Research Laboratories, Komenoki, Nissin, Aichi 470-0111, Japan

* E-Mail: photovoltaic2014@gmail.com

ABSTRACT

FeS_xO_y thin films were fabricated by the electrochemical deposition method on indium-tin-oxide(ITO)-coated glass substrates. FeS_xO_y is an environment-friendly material and is expected to have properties suitable for photovoltaics. The deposition solution contained $FeSO_4$ and $Na_2S_2O_3$. At 40ºC, a compact black film 0.5 μm in thickness with Fe:S:O composition 1:1:1 was deposited in 5 min on ITO substrate from a solution containing 40 mM $FeSO_4$ and 100 mM $Na_2S_2O_3$ at a pH 5.6 (inherent). In the photoelectrochemical measurement, the deposited FeS_xO_y film showed p-type conduction and photoconductivity. A ZnO/ FeS_xO_y heterostructure was fabricated, and rectification properties were confirmed.

Keywords: Iron sulfide, Iron oxide, Electrochemical Deposition, Heterojunction.

1. Introduction

Iron pyrite (FeS_2) is an attractive semiconducting material consisting of non-toxic and earth abundant elements. It is suitable as an absorber in a thin film solar cell owing to its large optical absorption coefficient of > 10^5 cm^{-1} in the near-infrared and visible light region [1,2]. Many methods have been used for the preparation of thin pyrite films, such as low pressure chemical vapor deposition [3], spray pyrolysis [4], sulfurization of electrodeposited films [5,6], sulfurization of sputtered [7] or vacuum evaporated [8,9] iron films, sol-gel [10,11], and chemical bath deposition [12]. More recently, use of ink technology was also reported, where precursor films of molecular inks composed of iron complexes and elemental sulfur were spin-coated and annealed [13]. The band gap of FeS_2 is considered to be 0.95 eV, which is in fact smaller than the optimum one for solar cells (about 1.5 eV [14]). Since Fe_2O_3 has a larger band gap (2.2 eV), one may expect that FeS_xO_y will have a larger band gap than FeS_2 and thus could be more suitable for photovoltaics [15]. However, the relation between the band gap and composition has not been investigated in details for FeS_xO_y. Several metal sulfide-oxide materials such as SnS_xO_y [16], $Cu_xSn_yS_zO$ [17] and Cu-Zn-Sn-S-O [18] have been fabricated by the electrochemical deposition (ECD) in our group. ECD is a cost-effective technique, and its advantage over other solution methods is the possibility of controlling film properties and thickness through the electrochemical variables. So far, there have been reports on the fabrication of FeS_xO_y by ECD [15] and photochemical deposition (PCD) [19]. While the conduction type was found to be n-type for the PCD FeS_xO_y film, the conduction type of the ECD film was not reported. Further, fabrication of heterostructure devices based on FeS_xO_y has never been attempted. Recently, Kawai et al. reported ECD of iron sulfide thin films and fabrication of pn heterojunction diodes based on ECD-iron sulfide [20]. In this work, we deposited FeS_xO_y thin films by ECD. In addition, a ZnO/FeS_xO_y heterostructure was fabricated, and rectification properties were confirmed.

2. Experiments

A three-electrode cell was used for ECD with a saturated calomel electrode (SCE) as the reference electrode. Indium-tin-oxide (ITO)-coated glass was used as the working electrode (substrate) and a platinum sheet was used as the counter electrode. Sheet resistance of ITO is 10 Ω/square. In the following, all the potential values are vs SCE.

Hokuto denko function generator HB-305 and potentiostat/galvanostat HA-151B were used as the voltage source. Both the ITO substrate and the platinum sheet were washed ultrasonically in alkyl benzene and dried in nitrogen before the experiment. The deposition area was about 1x1 cm^2. The deposition solution contained $FeSO_4$ (99.0 % purity) and 100 mM $Na_2S_2O_3$ (97.0 % purity). The deposition potential range was determined on the basis of the cyclic voltammetry. In order to investigate dependence of composition on various parameters, the deposition temperature was varied from 15 to 60ºC, the deposition potential from –0.8 to –1.0 V, and the $FeSO_4$ concentration from 20 to 40 mM. The solution pH was unadjusted, and the deposition time was 5 min. We obtained black films with a thickness ranging from 0.5 to 1.0 μm. (The thickness is larger for a more negative deposition potential.) After the deposition, the films were washed in pure water and naturally dried in air. Cracks were observed on the film surface by microscope observation for the deposition potentials more negative than –0.9 V, while adhesion to the substrate seemed good for potentials more positive than –0.9 V.

Iron sulfide is expected to be formed by the following mechanism, as reported for other sulfides. Elemental sulfur is released from $S_2O_3^{2-}$ by the reaction.

$$S_2O_3^{2-} + 2H^+ = S + H_2SO_3. \quad (1)$$

Then iron sulfide is formed at the cathode by the reaction

$$Fe^{2+} + xS + 2e^- = FeS_x. \quad (2)$$

For the oxide formation, one can consider dissolved oxygen and OH^- ions as the oxygen source. Since the solution is weakly acidic, the dominant oxygen source would be dissolved oxygen. Then iron oxide can be formed by the following reaction.

$$2Fe^{2+} + yO_2 + 4e^- = 2FeO_y. \quad (3)$$

With reactions (2) and (3) proceeding simultaneously, FeS_xO_y is expected to be formed.

Compositional analysis was carried out by Auger electron spectroscopy (AES) using a JEOL JAMP 9500 Auger microprobe at a probe voltage of 10 kV and a current of 10 nA. Argon ion etching with an acceleration voltage of 2.5 kV and a current of 8 mA was used to sputter the film surface. The scanning electron microscope (SEM) observation was also performed using JEOL JAMP 9500 at a constant acceleration voltage of 10 kV and a magnification of 5000. The film thickness was measured by an Accretech Surfcom-1400D profile meter. X-ray diffraction (XRD) was measured at the grazing-angle 3º of incident X ray using a Rigaku Smartlab diffractometer with a Cu Kα radiation source operated at 45

kV and 200 mA. The scan speed was 2º/min. The Raman spectra excited by a 632.8 nm He-Ne laser were collected using JASCO NRS 3300 spectrometer. The laser power was set low (0.9 mW), because high laser power could lead to decomposition of the deposited films. A JASCO U-570 ultraviolet/visible/near infrared spectrometer (a double-beam photometer) was used for optical transmission studies. We used the ITO substrate as the reference, and thus the absorption loss by ITO was corrected for. Furthermore, to determine the type of conduction and to estimate the photosensitivity, photoelectrochemical (PEC) measurements were carried out using the same potentiostat as used for the deposition. The three-electrode cell with a solution containing 100 mM $Na_2S_2O_3$ was used. The light was incident from a xenon lamp toward the backside of the sample. The incident light (about 100 mW/cm^2) was turned off and on mechanically every 5 s by inserting and removing a barrier between the lamp and the sample. This light chopping was performed under the application of a ramp voltage, first in the cathodic bias range (0 to -1 V) and then in the anodic bias range (0 to +1 V).

ZnO was also deposited by ECD using an aqueous solution containing 0.1 M $Zn(NO_3)_2$ (99.0 % purity) [21]. The deposition temperature was 60ºC. The deposition bias was a two-step pulse with V_1 = -1.3 V and V_2 = -0.6 V, and the duration of each pulse was 10s. The deposition time was 2 min, and the film thickness was about 0.5 μm. Indium was evaporated as electrodes on the ZnO/FeS_xO_y/ITO structure. Scanning-transmission electron microscope (STEM) observation was performed for the heterostructure using Hitachi High-Technologies HD-2700 at an acceleration voltage of 200 kV. The sample for cross-sectional observation was prepared by focused ion beam (FIB) milling with a protective film of carbon and molybdenum using Hitachi High-Technologies FIB system NB5000. The Ga ion milling source was operated at 30kV.

3. Results and Discussion

The elemental composition obtained by AES is shown in Figure 1 for the films deposited at different temperatures. The deposition potential was fixed at –0.8 V and the $FeSO_4$ concentration at 40 mM. The Fe content did not vary significantly and was in a range of 33~37 %. However, O and S contents depend strongly on the solution temperature. At 60ºC, sulfur precipitate were formed in the solution, and thus S content in the film was lower than that of films deposited at lower temperatures. Figure 2 shows the dependence of

elemental composition on the deposition potential. The deposition temperature was fixed at 40ºC and the $FeSO_4$ concentration at 40 mM. The composition did not depend significantly on the deposition potential. Figure 3 shows the results for different $FeSO_4$ concentrations with the temperature fixed at 15ºC and the potential at –1.0 V. The oxygen content increased with increasing $FeSO_4$ concentration. Nakamura et al. observed that S/Fe ratio of ECD-iron sulfide films is close to unity [6]. (The oxygen content in the films was not given in their paper.) The $FeSO_4$ concentration was fixed at 1 mM in their deposition. In our deposition, the $FeSO_4$ concentration is much larger, and this could be the reason for inclusion of large amount of oxygen since the oxygen content in the film tends to increase with increasing $FeSO_4$ concentration as shown in Fig.3. With the $FeSO_4$ concentration of 20 mM, S/Fe ratio is close to two, larger than in their results. The reason for this discrepancy is not understood.

In the deposition at 40ºC with deposition potential –0.8 V, $FeSO_4$ concentration 40 mM and pH 5.6 (unadjusted), a black film of 0.5 μm in thickness was obtained after 5 min. The elemental composition obtained for this film by AES is Fe:S:O ≈ 1:1:1 under that condition. Figure 4 shows the SEM image of the sample surface. The film is uniform and compact, with some surface roughness.

Figure 5 (a) shows the optical transmission spectrum of the FeS_xO_y film (5 min deposition). The optical transmission is lower than 10 %, and gradually increases with wavelength in a range from 800 to 1500 nm. Thus it seems difficult to determine the band gap energy from the transmission spectrum. The low transmission would mainly arise from light scattering due to surface roughness of the film. The origin of the small transmission peak at 750 nm is not understood. In fact, it was not observed for other samples, i.e., that part of the spectrum is not reproducible. We believe that it is not due to the interference effect, because the light scattering is strong with the surface being so rough. To reduce the effects of the roughness, we fabricated a thinner sample (0.3 μm thick) by reducing the deposition time to 3 min. Figure 5 (b) shows the optical transmission spectrum for that thinner film. The transmission is larger than in Fig.5(a), but a clear absorption edge is not observed. There is a gradual drop near 950 nm in both Figs.5 (a) and (b), and this drop may correspond to the band gap (about 1.3 eV). However, the drop is so gradual that the band gap value cannot be determined conclusively. The spectra in Fig.5 are not significantly different from that observed for iron sulfide deposited by the same technique, which has

much reduced oxygen content [20], and therefore we are unable to confirm any widening of the band gap due to substitution of sulfur with oxygen.

Figure 6 shows the PEC measurement results for the FeS_xO_y films. The photo-response was observed in both the polarity, but the negative photocurrent under the negative bias is higher than the positive photocurrent under the positive bias. Accordingly, the film would be a p-type semiconductor.

Figure 7 shows the grazing-incidence XRD pattern measured for the FeS_xO_y film grown on the ITO substrate. All the observed diffraction peaks are attributed to ITO, and thus the FeS_xO_y film is considered to be amorphous. On the other hand, since there are no peaks due to elemental Fe, we can conclude that Fe is chemically bonded to S or O.

Figure 8 shows the Raman spectrum of the FeS_xO_y thin film with the spectra for hematite (α-Fe_2O_3) and pyrite (FeS_2) shown for comparison. If deposited FeS_xO_y is a composite of iron oxides and sulfides (i.e., Fe is bonded to either O only or S only), then the peaks for iron oxides and sulfides will be observed. However, the peak frequencies for FeS_xO_y (249 and 305 cm^{-1}) are distinctly different from those for α-Fe_2O_3 or FeS_2, as shown in Fig.8. Marcasite (FeS_2) has dominant peaks around 325 and 385 cm^{-1}, similar to pyrite peaks P1 and P2 in Fig.8, and pyrrhotite (Fe_7S_8) peaks are at 320-340 and 370 cm^{-1} [22]. Recently, Bi et al. reported that FeS has Raman peaks at 210 and 280 cm^{-1} and amorphous $Fe_{1-x}S$ at 152, 292, and 354 cm^{-1} [23]. Vequizo et al. found that γ-FeOOH can be deposited by ECD, and that the dominant Raman peaks were at 250 and 385 cm^{-1} [24]. Other FeOOH phases have the most dominant peak around 400 cm^{-1}. One of the dominant peak of FeS_xO_y (F1) has almost the same frequency as one of the peaks of γ-FeOOH (250 cm^{-1}), but the other dominant peak of γ-FeOOH (385 cm^{-1}) was not observed for FeS_xO_y. Thus the Raman spectrum for FeS_xO_y does not match with any of the spectra of those other oxide and sulfide phases. Therefore, we may consider that Fe atoms in FeS_xO_y are bonded to both O and S atoms so that new vibrational bands are formed.

The cross-sectional STEM photograph of the ZnO/FeS_xO_y heterostructure is shown in Fig. 9. Although the interface is not flat, the two-layer structure can be clearly seen. The FeS_xO_y film thickness obtained from Fig. 9 is 0.3 - 0.4 μm, slightly smaller than that obtained for a single layer by the profile meter (about 0.5 μm). The ZnO thickness seems to be about 0.6 μm. Figure 10 shows the results of the current-voltage (I-V) measurement in the dark for the ZnO/FeS_xO_y heterostructure. In the figure, the positive voltage means

that the FeS_xO_y side of the sample was positively biased with respect to the ZnO side. Thus, this result shows that an n-ZnO/p-FeS_xO_y rectifying junction was formed. The leakage current is about $1x10^{-2}$ mA/cm^2 at -1.0 V. We also measured I-V curves for In/FeS_xO_y/ITO and In/ZnO/ITO structures, and found that they showed ohmic properties. Thus the rectification takes place in the ZnO/ FeS_xO_y junction.

4. Conclusion

In this work, FeS_xO_y thin films were deposited by the ECD method from the deposition solution containing $FeSO_4$ and $Na_2S_2O_3$. The composition obtained by AES was Fe:S:O ≈ 1:1:1, when the $FeSO_4$ concentration was 40 mM, $Na_2S_2O_3$ concentration 100 mM, and the deposition temperature 15 ~ 40ºC. By the PEC measurement, a negative photocurrent was observed under illumination, and thus the film was considered to be p-type. A ZnO/ FeS_xO_y heterostructure was fabricated, and in the current-voltage measurement, clear rectification properties were observed.

References

[1] A. Ennaoui, S. Fiechter, W. Jaegermann, H. Tributsch, Photoelectrochemistry of Highly Quantum Efficient Single-Crystalline n-FeS_2 (Pyrite), J. Electrochem. Soc. 133 (1986) 97-106.

[2] A. Ennaoui, S. Fiechter, C. Pettenkofer, N. Alonsovante, K. Buker, M. Bronold, C. Hopfner, H. Tributsch, Iron disulfide for solar energy conversion, Sol. Energy Mater. Sol. Cells 29 (1993) 289-370.

[3] D.M. Schleich, H.S.W. Chang, Iron pyrite and iron marcasite thin films prepared by low pressure chemical vapor deposition, J. Cryst. Growth 112 (1991) 737-744.

[4] A. Yamamoto, M. Nakamura, A. Seki, E.L. Li, A. Hashimoto, S. Nakamura, Pyrite (FeS_2) thin films prepared by spray method using $FeSO_4$ and $(NH_4)_2S_x$, Sol. Energy Mater. Sol. Cells 75 (2003) 451-456.

[5] G. Pimenta, W. Kautek, Pyrite film formation by H_2S reactive annealing of iron, Thin Solid Films 238 (1994) 213-217.

[6] S. Nakamura, A. Yamamoto, Electrodeposition of pyrite (FeS_2) thin films for photovoltaic cells, Sol. Energy Mater. Sol. Cells 65 (2001) 79-85.

[7] L. Meng, J.P. Tu, M.S. Liu, Formation of pyrite thin films by sulfidation annealing of iron films, Mater. Lett. 38 (1999) 103-107.

[8] B. Rezig, H. Dahman, M. Kenzari, Iron pyrite FeS_2 for flexible solar cells, Renewable Energy 2 (1992) 125-128.

[9] I.J. Ferrer, C. Sanchez, Characterization of FeS_2 thin films prepared by thermal sulfidation of flash evaporated iron, J. Appl. Phys. 70 (1991) 2641-2647.

[10] H. Siyu, L. Xinyu, L. QingYu, C. Jun, Pyrite film synthesized for lithium-ion batteries, J. of Alloys and Comp. 472 (2009) L9-L12.

[11] L. Huang, F. Wang, Z. Luan, L. Meng, Pyrite (FeS_2) thin films deposited by sol–gel method, Materials Letters 64 (2010) 2612-2615.

[12] D. A. Mazon-Montijo, M. T. S. Nair, P. K. Nair, Iron Pyrite Thin Films via Thermal Treatment of Chemically Deposited Precursor Films, Journal of Solid State Science and Technology 2 (11) (2013) P465-470.

[13] S. Seefeld, M. Limpinsel, Y. Liu, N. Farhi, A. S. Weber, Y. Zhang, N. Berry, Y. J. Kwon, C. L. Perkins, J. C. Hemminger, R. Wu, M. Law, Iron Pyrite Thin Films

Synthesized from an $Fe(acac)_3$ Ink, J. Am. Chem. Soc. 135 (2013) 4412-4424.

[14] J.J. Loferski, Theoretical ConSiderations Governing the Choice of the Optimum Semiconductor for Photovoltaic Solar Energy Conversion, J. Appl. Phys. 27 (1956) 777-781.

[15] X. Han, B. Zhou, M. Tao, Earth-Abundant Iron Oxysulfide (FeS_xO_y) for Bandgap Optimization, 38th IEEE Photovoltaic Specialists Conference (PVSC), (2011) 002528-002532.

[16] K. Omoto, N. Fathy, M. Ichimura, Deposition of SnS_xO_y Films by Electrochemical Deposition Using Three-Step Pulse and Their Characterization, Jpn. J. Appl. Phys. 45 (2006) 1500-1505.

[17] Y. Nakashima, M. Ichimura, Electrochemical Deposition of $Cu_xSn_yS_zO$ Thin Films and Their Application for Heterojunction Solar Cells, Inter. J. Photoenergy 2012 (2012) 171432 1-8.

[18] K. Yang, M. Ichimura, Fabrication of Cu–Zn–Sn–S–O Thin Films by the Electrochemical Deposition Method and Application to Heterojunction Cells, Inter. J. Photoenergy 2012 (2012) 154704 1-6.

[19] H. R. Dizaji, M. Ichimura, Photochemical deposition of FeS_xO_y, Mater. Sci. Eng. B 158 (2009) 26-29.

[20] S. Kawai, R. Yamazaki, S. Sobue, E. Okuno, and M. Ichimura, Electrochemical deposition of iron sulfide thin films and heterojunction diodes with zinc oxide , APL Matter. 2 (2014) 032108.

[21] M. Izaki, T. Omi, Electrolyte Optimization for Cathodic Growth of Zinc Oxide Films, J. Electrochem. Soc. 143 (1996) L53-L55.

[22] The RRUFF Project (http://rruff.info/)

[23] Y. Bi, Y. Yuan, C. L. Exstrom, S. A. Darveau, and J. Huang, Air Stable, Photosensitive, Phase Pure Iron Pyrite Nanocrystal Thin Films for Photovoltaic Application, Nano Lett. 11 (2011) 4953-4957.

[24] J. J. M. Vequizo and M. Ichimura, Electrodeposition and Characterization of γ-FeOOH Thin Films from Oxygen-Bubbled Aqueous Iron Sulfate Solutions, Appl. Phys. Express, 6 (2013) 125501.

Fig. 1. Composition of FeS_xO_y films deposited at different temperatures. (The potential was –0.8 V, and the $FeSO_4$ concentration 40mM)

Fig. 2. Composition of FeS_xO_y films deposited at different potentials. (The temperature was 40ºC, and the $FeSO_4$ concentration 40 mM)

Fig. 3. Composition of FeS_xO_y films deposited with different $FeSO_4$ concentrations. (The temperature was 15ºC, and the potential -1.0V)

Fig. 4. SEM photograph of the surface of the FeS_xO_y film.

Fig. 5. Optical transmission spectra for the FeS_xO_y films. (a): 5 min deposition. (b) 3 min deposition.

Fig. 6. PEC measurement results of the FeS_xO_y film.

Fig. 7. Grazing-incidence X-ray diffraction pattern of the FeS_xO_y film on the ITO substrate.

Fig. 8. Raman spectra of FeS_xO_y, hematite (α-Fe_2O_3), and pyrite (FeS_2).

Fig.9. STEM cross sectional view of the ZnO/ FeS_xO_y / ITO heterojunction.

Fig. 10. Current-voltage characteristics of the ZnO/ FeS_xO_y / ITO heterojunction cell.

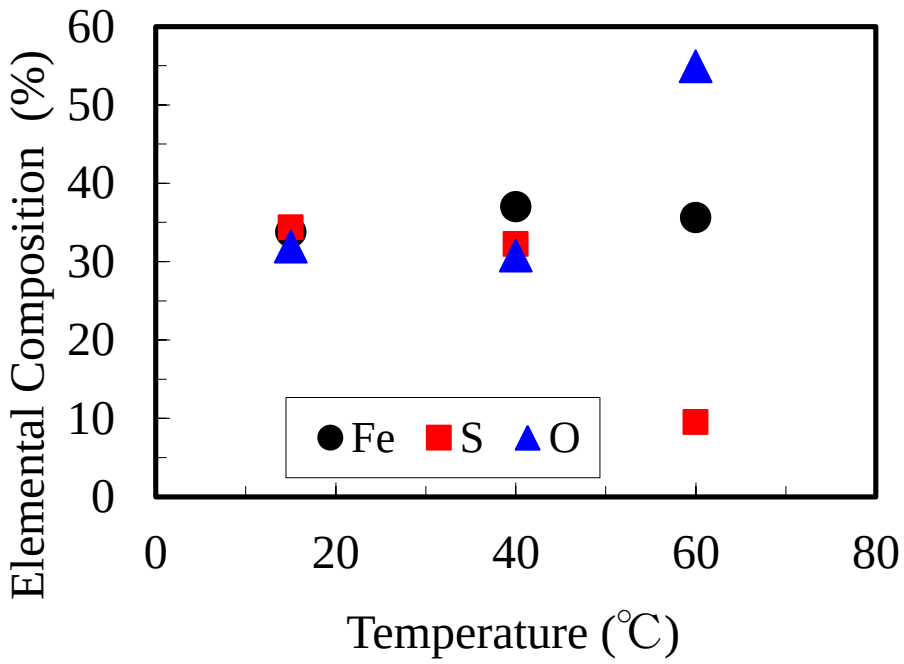
Elemental Composition (%)
60
50
40
30
20
10
0
0
20
40
60
80
Temperature (℃)
Fe
S
O

Fig.1

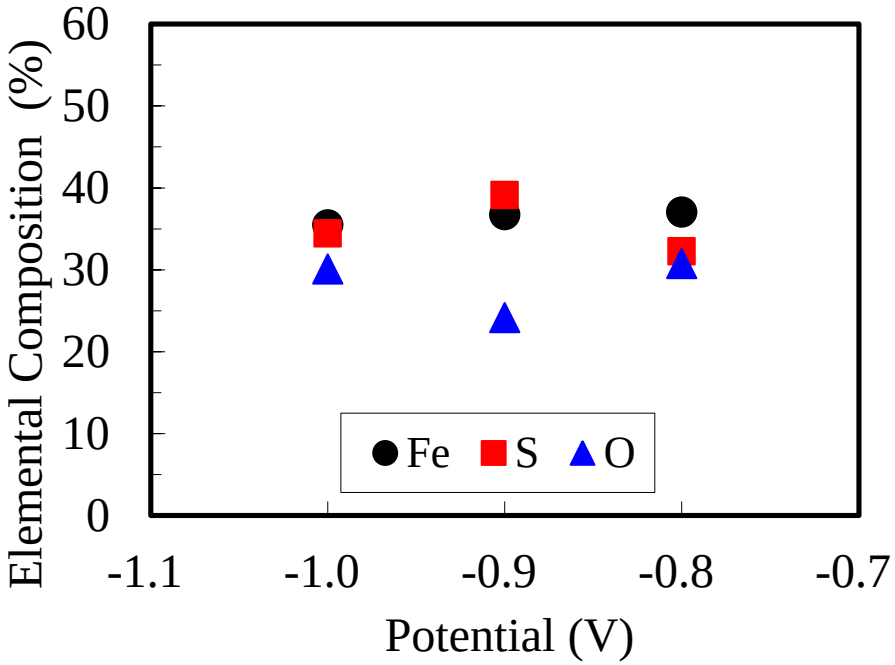
Elemental Composition (%)
60
50
40
30
20
10
0
-1.1
-1.0
-0.9
-0.8
-0.7
Potential (V)
Fe
S
O

Fig.2

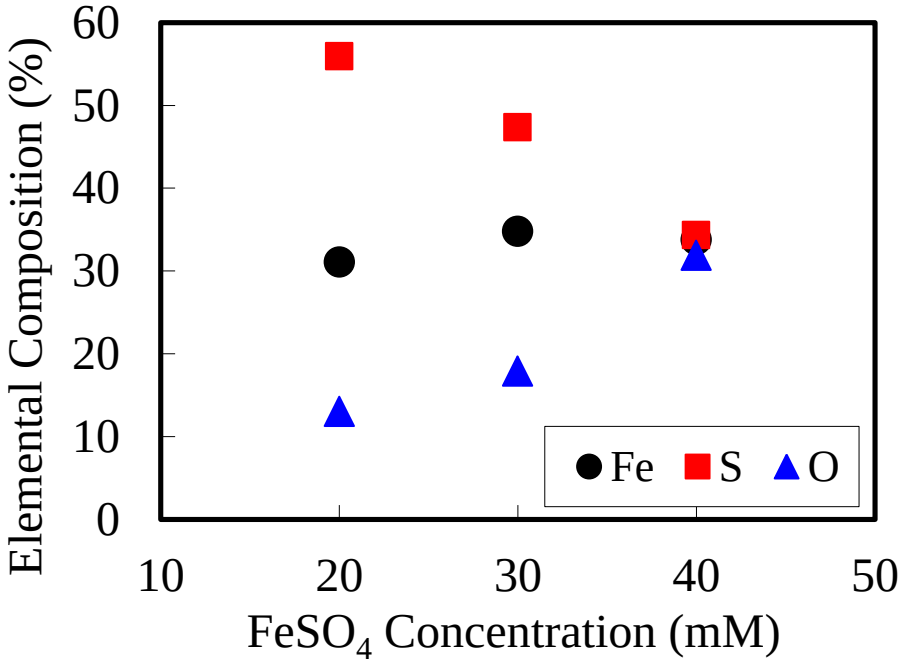
Elemental Composition (%)
60
50
40
30
20
10
0
10
20
30
40
50
FeSO4 Concentration (mM)
Fe
S
O

Fig.3

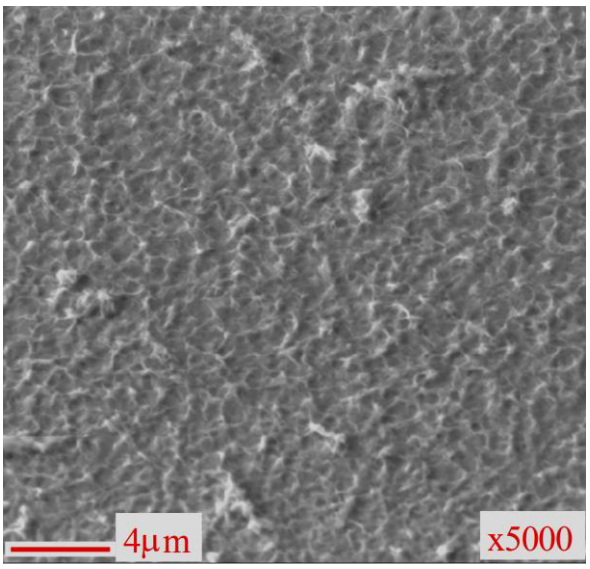

Fig.4

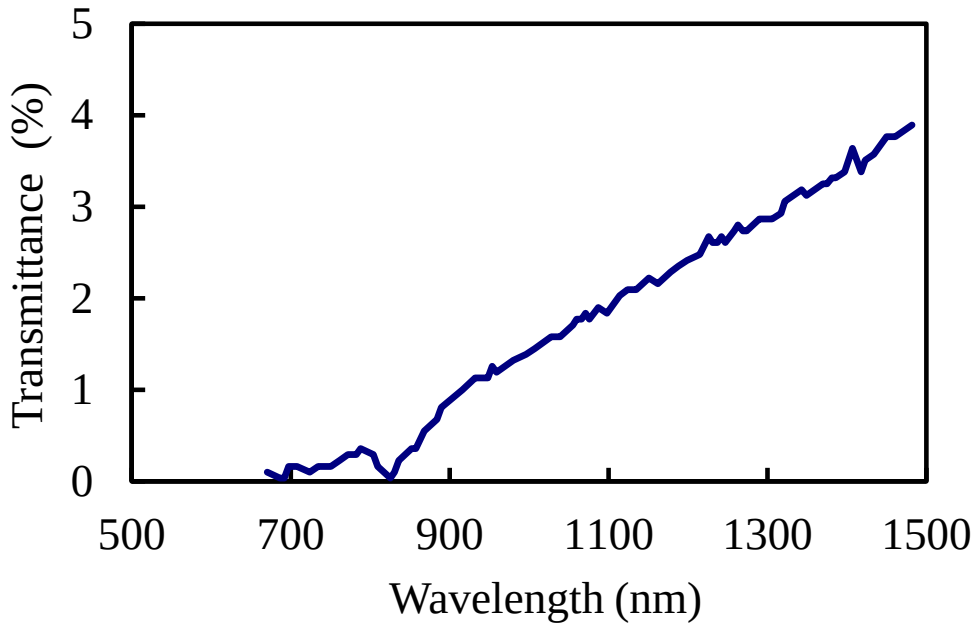
Transmittance (%)
0
1
2
3
4
5
500
700
900
1100
1300
1500
Wavelength (nm)

(a)

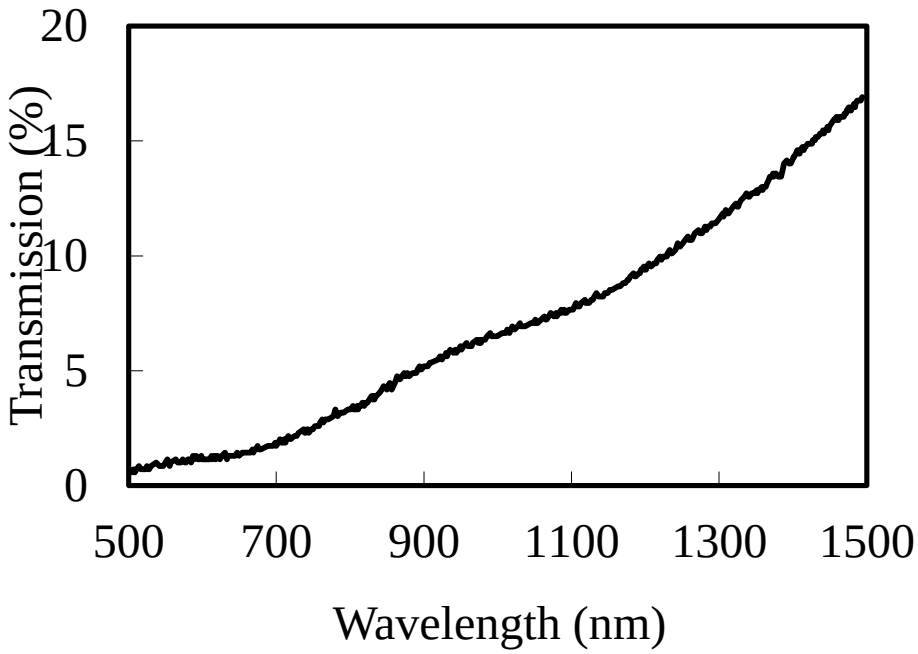
Transmission (%)
0
5
10
15
20
500
700
900
1100
1300
1500
Wavelength (nm)

(b)

Fig.5

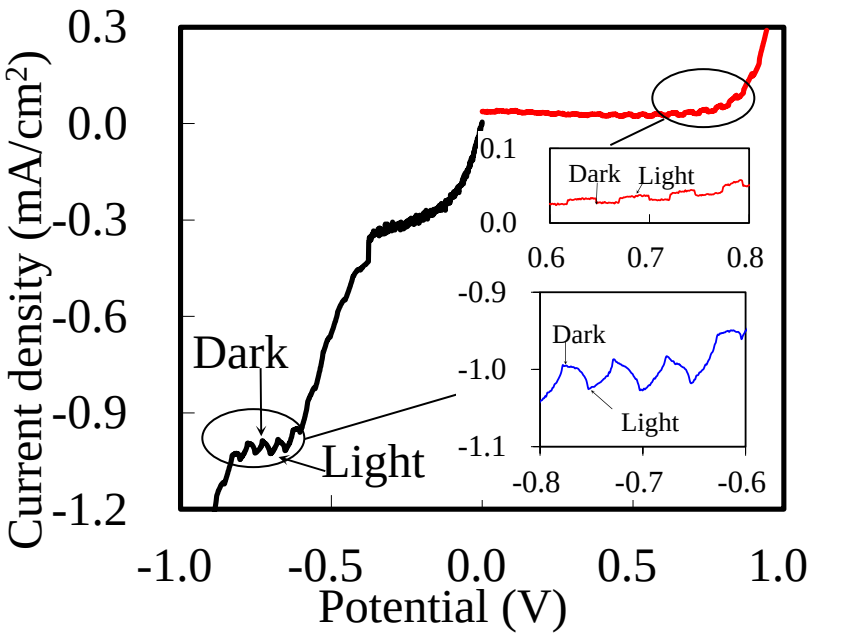
Current density (mA/cm²)
0.3
0.0
-0.3
-0.6
-0.9
-1.2
-1.0
-0.5
0.0
0.5
1.0
Potential (V)
Dark
Light
0.1
0.0
0.6
0.7
0.8
Dark
Light
-0.9
-1.0
-1.1
-0.8
-0.7
-0.6
Dark
Light

Fig.6

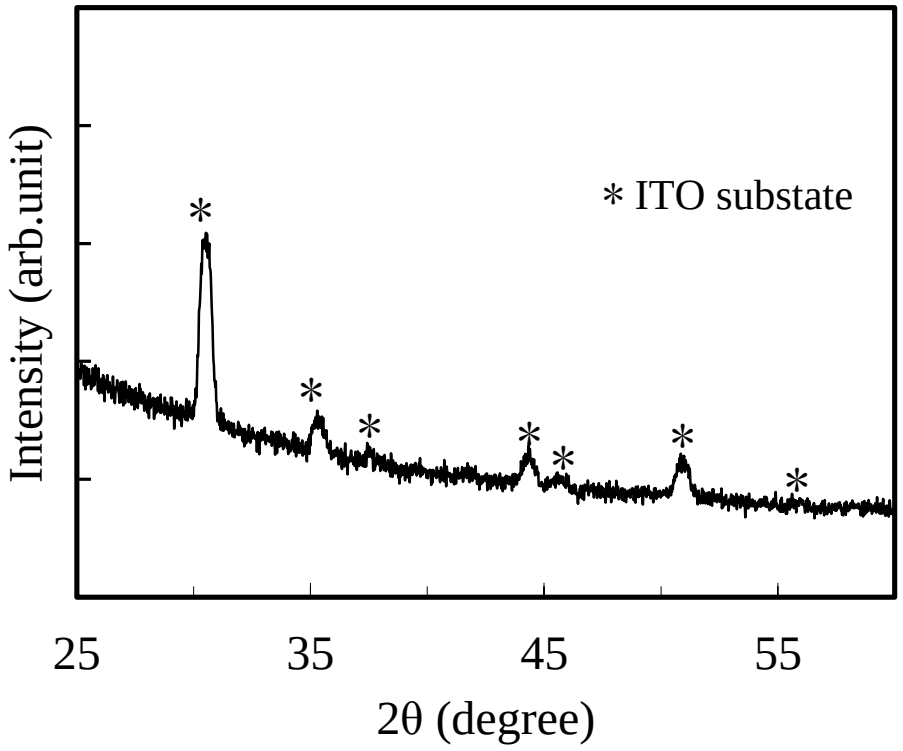

Fig.7

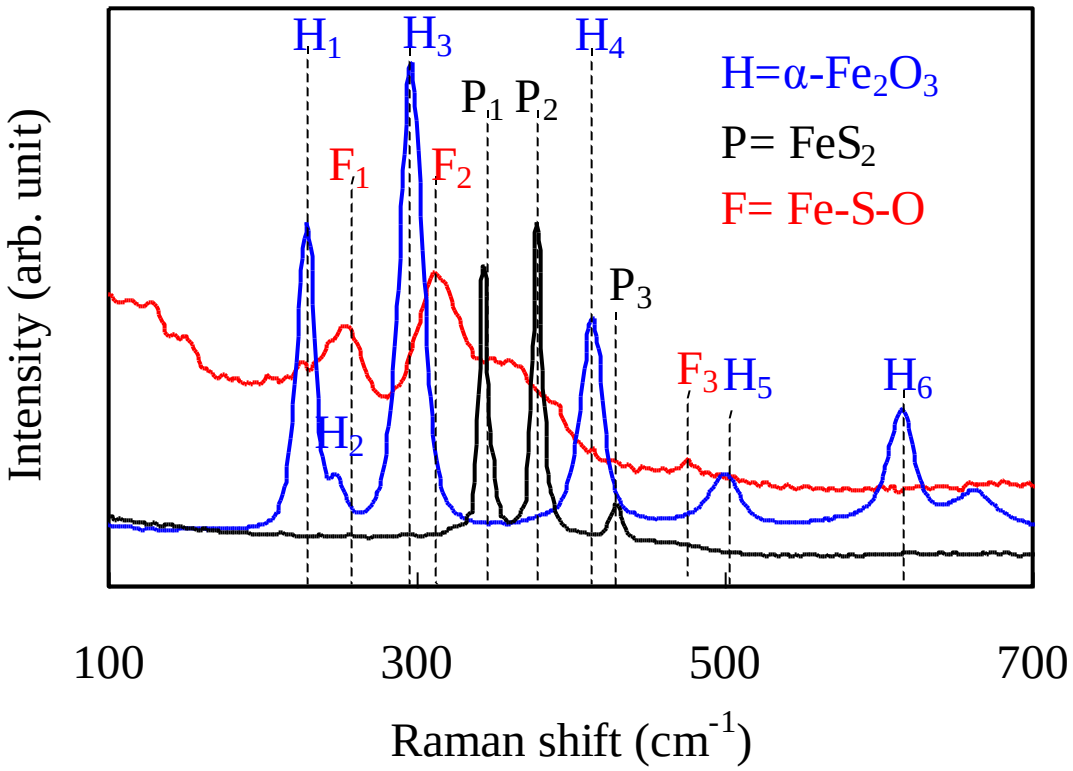
H1
H3
H4
P1 P2
H=α-Fe2O3
P= FeS2
F= Fe-S-O
F1
F2
P3
F3 H5
H6
H2
Intensity (arb. unit)
100
300
500
700
Raman shift (cm-1)

Fig.8

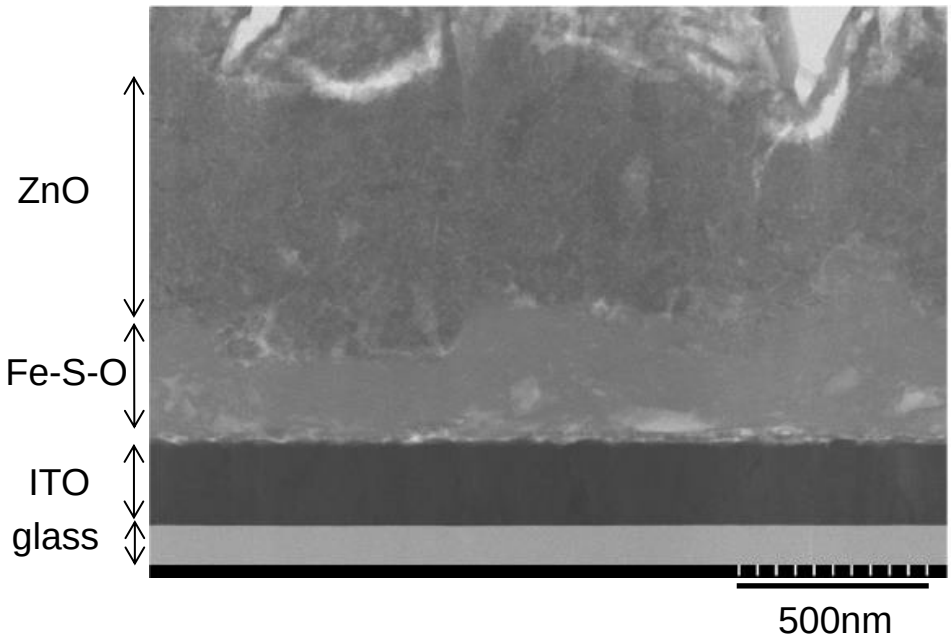

Fig.9

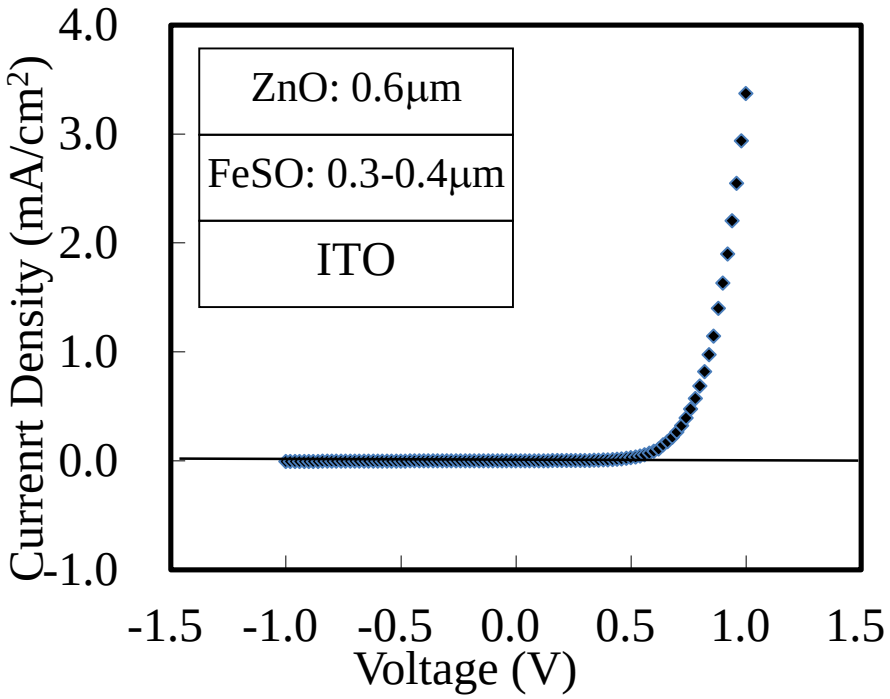
4.0
3.0
2.0
1.0
0.0
-1.0
Currenrt Density (mA/cm²)
ZnO: 0.6μm
FeSO: 0.3-0.4μm
ITO
-1.5
-1.0
-0.5
0.0
0.5
1.0
1.5
Voltage (V)

Fig.10